

# Theoretical Study and Parameter Optimization of CFST Pillar in Cooling Tower

Xiaoxiong Zha\*, Peichang Xu, and Dejin Chen

School of Civil and Environment Engineering, Shenzhen Graduate School, Harbin Institute of Technology, Shenzhen, China

## Abstract

The application of concrete pillar in cooling towers has become more common. However, the CFST (Concrete Filled Steel Tube) pillar has no relevant applications and researches in cooling towers. In order to research the CFST pillar, we will analyze the optimization of the parameters of the CFST pillar first. In CFST pillar, the parameters that can be optimized are: The position of the intersection (above, below, or in the middle), the cross angle, the tilt angle of the CFST pillar, the form of the intersection, the form of the pillar section, etc. Changes in these parameters can also cause a large change in the CFST pillar internal force. The purpose of this paper is to obtain the optimal value range of "intersection position, cross angle, and CFST pillar tilt angle" in the CFST pillar parameters through theoretical calculations, and to provide parameters selection suggestions for cooling tower engineering design. The main theories adopted are: classical structural mechanics (e.g., force method, displacement method, moment distribution method, graph multiplication, etc.), moment distribution method of space rigid frame, and transformation rule of space coordinates. We analyze the CFST pillar by three-dimensional structural mechanics and use MatLab to obtain the optimized results of CFST pillar parameters.

**Keywords:** CFST pillar; Structural mechanics; MatLab; Intersection; Configuration; Horizontal; Load

## Background

The parameters related to the construction of the CFST X-pillar include: the cross angle of the CFST X-pillar is  $\alpha$ , the angle between the pillar and the ground is  $\beta$ , the length of the pillar is  $L$ , and the distance between the pillar intersection and the upper end is  $\lambda L$ .

This article will use the method of classical structural mechanics, combined with the transformation rules of spatial coordinates, to derive the CFST X-pillar internal force calculation formula and then use calculation formula to optimize the parameters of CFST X-pillars.

This paper only considers the static load of the CFST X-pillar, mainly including the gravity load  $G$  of the superstructure, and the equivalent static wind load  $P$  (Figure 1).

## Structural Analysis

### Load analysis

**Gravity load distribution:** CFST X-pillars are generally spaced at regular intervals, then the gravity load  $G$  will be evenly distributed to each CFST X-pillar. Suppose that the number of CFST X-pillars in the cooling tower is  $n$ , then  $G_1 = G_2 = \dots = G_m = \dots = G_n$  (Figure 2).

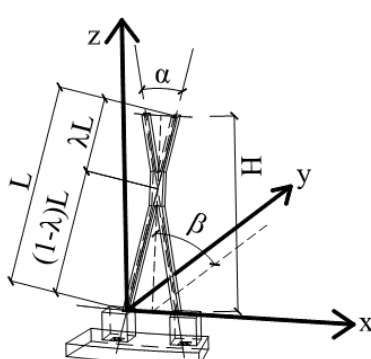


Figure 1: CFST X-pillar configuration parameters.

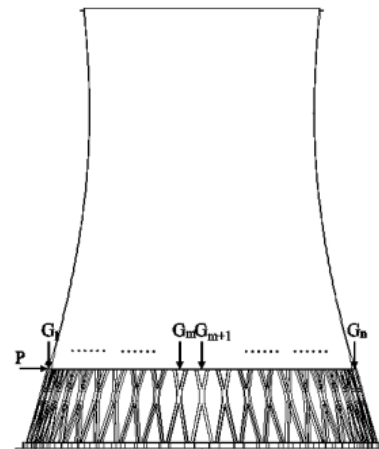


Figure 2: Cooling tower overall model.

**Corresponding author:** Xiaoxiong Zha, School of Civil and Environment Engineering, Shenzhen Graduate School, Harbin Institute of Technology, Shenzhen, China, Tel: +86-158-1685-3765; E-mail: [zhahero@126.com](mailto:zhahero@126.com)

**Received** November 19, 2017; **Accepted** November 26, 2018; **Published** December 03, 2018

**Citation:** Zha X, Xu P, Chen D (2018) Theoretical Study and Parameter Optimization of CFST Pillar in Cooling Tower. J Steel Struct Constr 4: 148. doi: [10.4172/2472-0437.1000148](https://doi.org/10.4172/2472-0437.1000148)

**Copyright:** © 2018 Zha X, et al. This is an open-access article distributed under the terms of the Creative Commons Attribution License, which permits unrestricted use, distribution, and reproduction in any medium, provided the original author and source are credited.

beam will move in its entirety, and it will also bring about the same horizontal displacement  $\Delta_p$  at the top of all CFST X-pillars. Suppose the CFST X-pillar closest to the horizontal load  $P$  is the first pillar. Counterclockwise, the lateral stiffness of the  $i$ -th CFST X-pillar is  $K_{Si}$  and the horizontal load it is assigned to is  $P_i$ .

There is the equation,  $\Delta_p = \frac{P_1}{K_{S1}} = \frac{P_2}{K_{S2}} = \dots = \frac{P_n}{K_{Sn}}$ .

Therefore, the load distribution value of the horizontal load  $P$  at the top of each CFST X-pillar is determined according to the ratio between  $K_{Si}$ . In addition, the lateral stiffness  $K_s$  of the X pillar is mainly composed of two parts: the in-plane stiffness  $K_{in}$  and the out-of-plane stiffness  $K_{out}$  (Figure 4) the in-plane stiffness is  $K_{in}$  along the x-direction, and the out-of-plane stiffness is  $K_{out}$  along the y-direction.

Similarly, the horizontal load  $P$  can be decomposed into an in-plane horizontal load  $P_{in}$  and an out-plane horizontal load  $P_{out}$ . The final load condition of a single CFST X-pillar can be represented as shown in Figure 5.

Conclusion: In order to obtain the lateral stiffness  $K_s$  in any direction of the CFST X-pillar, the in-plane rigidity  $K_{in}$  and the out-of-plane stiffness  $K_{out}$  of the CFST X-pillar are required to be calculated. And then according to  $K_s$ , the load distribution of the horizontal load  $P$

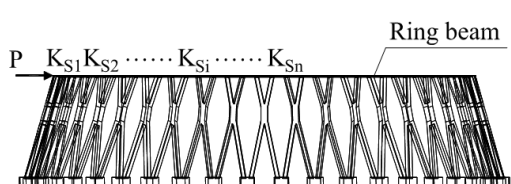


Figure 3: A rigid frame model consisting of CFST X-pillars and a ring beam.

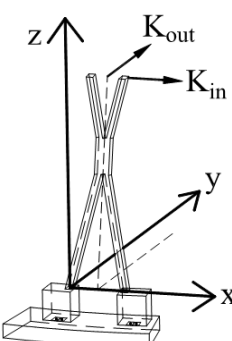


Figure 4: In-plane stiffness and Out-of-plane stiffness of CFST X-pillar.

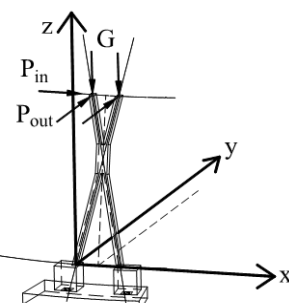


Figure 5: CFST X-pillar load conditions.

at the top of each CFST X-pillar can be obtained in the overall structure.

### Boundary condition analysis

When the stiffness of the ring beam is assumed to be infinite, the boundary condition at the top of the CFST X-pillar can be considered as the slip bearing (Figure 6).

### Basic assumption

Basic assumptions for theoretical analysis in this paper:

- The ring beam above the CFST X-pillars does not allow large deformations. So it can be assumed to be a rigid body.
- Suppose  $EA=\infty$  in the analysis of internal forces.

### In-plane Stiffness $K_{in}$ (Two-dimensional calculation)

According to the simplified calculation model, the X pillar is fixed at the bottom and the top of it is the sliding bearing. Because the force and deformation of the CFST X-pillars are both in-plane, the calculation of the in-plane stiffness  $K_{in}$  can be reduced to a two-dimensional problem (Figure 7).

AECD is a CFST X-pillar with intersection B. Points C and E are sliding bearings. Points A and D are fixed bearings. A rigid body CE is connected between points C and E at the top of the pillar. The length of the CD is L.  $CB/CD=\lambda$ . The load of the pillar can be equivalent as shown in Figure 8.

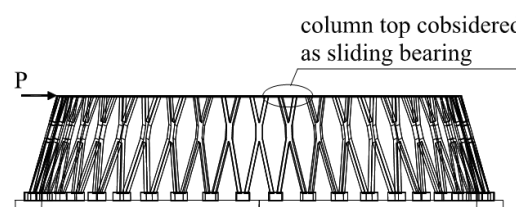


Figure 6: CFST X-pillar boundary condition.

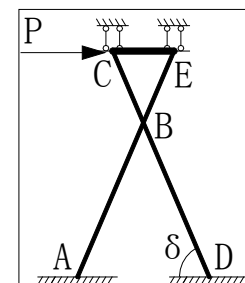


Figure 7: CFST X-pillar in-plane stiffness calculation model.

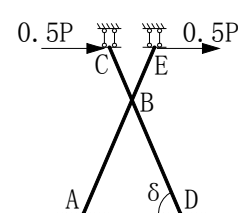


Figure 8: CFST X-pillar in-plane stiffness equivalent model.

The expression of internal force of bending moment can be obtained by moment distribution method and displacement method [1]. Here only the internal force of the BC rod end is given:

$$M_{BC}^{P_{in}} = -\frac{\eta_{in}(7-3\lambda)\lambda^2 LP_{in}}{4(1+3\lambda)} - \frac{(1-\lambda)^2 LP_{in}}{4\cos\frac{\alpha}{2}}$$

$$\eta_{in} = \cos\frac{\alpha}{2} - \frac{(A\lambda^2 L^2 - 12I)\sin\frac{\alpha}{2}}{A\lambda^2 L^2 \tan\frac{\alpha}{2} + 12I \cot\frac{\alpha}{2}}$$

Then calculate the internal force of the bending moment of the basic structure under the force of unit "1". Here only the internal force of the BC rod end is given:

$$\bar{M}_{BC}^1 = -0.5L_{CB}\cos\frac{\alpha}{2} = -\frac{1}{2}\lambda L\cos\frac{\alpha}{2}$$

Finally, CFST X-pillar top displacement  $\Delta_{in}$  can be obtained by the method of graph multiplication under in-plane force  $P_{in}$ :

$$\Delta_{in} = \sum \int \frac{\bar{M}_i M_p}{EI} = \frac{\eta_{in}(12\lambda^2 - 70\lambda + 34)\lambda^3 L^3 P_{in} \cos\frac{\alpha}{2}}{48(1+3\lambda)EI} + \frac{1}{24EI}(1-2\lambda)(1-\lambda)^2 \lambda L^3 P_{in}$$

So the in-plane stiffness is,  $K_{in} = \frac{1}{\Delta_{in}}$ .

## Moment Distribution Method for Space Rigid Frames

When calculating the out-of-plane bending stiffness  $K_{out}$  of the CFST X-pillar, we should use the moment distribution method for space rigid frames. Regarding to the moment distribution method for space rigid frames, Xiling Ma et al. has done relevant research [2]. Their research results are only suitable when structural members are perpendicular to each other. Here we will use the law of spatial coordinate transformation to derive the case for structural members that are not perpendicular to each other.

As shown in Figure 9,  $O'x'y'z'$  is the local coordinate system and  $Oxyz$  is the global coordinate system. The angular displacement components of the member  $ij$  in the local coordinate system are:  $\theta_{x'i}$ ,  $\theta_{y'i}$ ,  $\theta_{z'i}$ ,  $\theta_{x'j}$ ,  $\theta_{y'j}$ ,  $\theta_{z'j}$ . Among them,  $\theta_{x'i}$  and  $\theta_{x'j}$  are the twist angles of the member, and  $\theta_{y'i}$ ,  $\theta_{y'j}$  and  $\theta_{z'i}$ ,  $\theta_{z'j}$  are the rotation angles of the end surfaces around the  $y$ -axis and the  $z$ -axis, respectively, when the member  $ij$  is bent. Figure 10 shows the six moments acting on the ends of the member in the local coordinate system:  $M_{ij}^{x'}$ ,  $M_{ij}^{y'}$ ,  $M_{ij}^{z'}$ ,  $M_{ji}^{x'}$ ,  $M_{ji}^{y'}$ ,  $M_{ji}^{z'}$ . Among them,  $M_{ij}^{y'}$ ,  $M_{ji}^{y'}$  are torques;  $M_{ij}^{x'}$ ,  $M_{ji}^{x'}$  and  $M_{ij}^{z'}$ ,  $M_{ji}^{z'}$  are bending moments about the  $y$ -axis and the  $z$ -axis, respectively. In addition, the above-mentioned angular displacement and couple moment vector are positive in the positive direction of the coordinate axis according to the right-handed helix rule [3].

Figure 9: Member end angular displacement in local coordinate system.

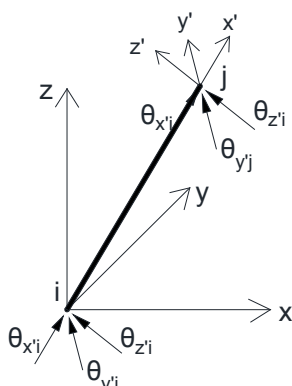


Figure 9: Member end angular displacement in local coordinate system.

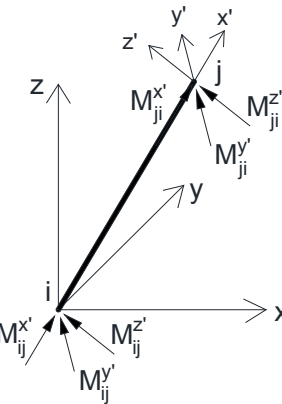


Figure 10: Member end moment in local coordinate system.

$M_{ij}^{z'}$  are bending moments about the  $y$ -axis and the  $z$ -axis, respectively. In addition, the above-mentioned angular displacement and couple moment vector are positive in the positive direction of the coordinate axis according to the right-handed helix rule [3].

The stiffness matrix of the member  $ij$  in the local coordinate system is:

$$\begin{bmatrix} M_{ij}^{x'} \\ M_{ij}^{y'} \\ M_{ij}^{z'} \\ M_{ji}^{x'} \\ M_{ji}^{y'} \\ M_{ji}^{z'} \end{bmatrix} = \frac{1}{L} \begin{bmatrix} GI_t & 0 & 0 & -GI_t & 0 & 0 \\ 0 & 4EI_y & 0 & 0 & 2EI_y & 0 \\ 0 & 0 & 4EI_z & 0 & 0 & 2EI_z \\ -GI_t & 0 & 0 & GI_t & 0 & 0 \\ 0 & 2EI_y & 0 & 0 & 4EI_y & 0 \\ 0 & 0 & 2EI_z & 0 & 0 & 4EI_z \end{bmatrix} \begin{bmatrix} \theta_{x'i} \\ \theta_{y'i} \\ \theta_{z'i} \\ \theta_{x'j} \\ \theta_{y'j} \\ \theta_{z'j} \end{bmatrix}$$

Marked as:  $M' = K'\theta'$ ;

Let the relationship between the local coordinate system and the global coordinate system be:

$$\begin{cases} l_{11} = \cos\langle x, x' \rangle & l_{21} = \cos\langle y, x' \rangle & l_{31} = \cos\langle z, x' \rangle \\ l_{12} = \cos\langle x, y' \rangle & l_{22} = \cos\langle y, y' \rangle & l_{32} = \cos\langle z, y' \rangle \\ l_{13} = \cos\langle x, z' \rangle & l_{23} = \cos\langle y, z' \rangle & l_{33} = \cos\langle z, z' \rangle \end{cases}$$

The conversion matrix from the local coordinate system to the global coordinate system is:

$$T = \begin{bmatrix} l_{11} & l_{12} & l_{13} & 0 & 0 & 0 \\ l_{21} & l_{22} & l_{23} & 0 & 0 & 0 \\ l_{31} & l_{32} & l_{33} & 0 & 0 & 0 \\ 0 & 0 & 0 & l_{11} & l_{12} & l_{13} \\ 0 & 0 & 0 & l_{21} & l_{22} & l_{23} \\ 0 & 0 & 0 & l_{31} & l_{32} & l_{33} \end{bmatrix}$$

In the global coordinate system, there are:  $M = K$ ;  $M = TM$ ;  $\theta = T\theta'$

$$So, M = T K' T^T; K = T K' T^T$$

The global stiffness matrix is:

$$K = \begin{bmatrix} l_{11} & l_{12} & l_{13} & 0 & 0 & 0 \\ l_{21} & l_{22} & l_{23} & 0 & 0 & 0 \\ l_{31} & l_{32} & l_{33} & 0 & 0 & 0 \\ 0 & 0 & 0 & l_{11} & l_{12} & l_{13} \\ 0 & 0 & 0 & l_{21} & l_{22} & l_{23} \\ 0 & 0 & 0 & l_{31} & l_{32} & l_{33} \end{bmatrix} \times \frac{1}{L} \begin{bmatrix} GI_t & 0 & 0 & -GI_t & 0 & 0 \\ 0 & 4EI_y & 0 & 0 & 2EI_y & 0 \\ 0 & 0 & 4EI_z & 0 & 0 & 2EI_z \\ -GI_t & 0 & 0 & GI_t & 0 & 0 \\ 0 & 2EI_y & 0 & 0 & 4EI_y & 0 \\ 0 & 0 & 2EI_z & 0 & 0 & 4EI_z \end{bmatrix} \times \begin{bmatrix} l_{11} & l_{21} & l_{31} & 0 & 0 & 0 \\ l_{12} & l_{22} & l_{32} & 0 & 0 & 0 \\ l_{13} & l_{23} & l_{33} & 0 & 0 & 0 \\ 0 & 0 & 0 & l_{11} & l_{12} & l_{13} \\ 0 & 0 & 0 & l_{21} & l_{22} & l_{23} \\ 0 & 0 & 0 & l_{31} & l_{32} & l_{33} \end{bmatrix} =$$

$$\begin{bmatrix} \frac{1}{L} & & & & & & & \\ & GLJ_{11}^2 + 4EI_J_{11}^2 + 4EI_J_{12}^2 & GLJ_{12}^2 + 4EI_J_{12}^2 + 4EI_J_{22}^2 & & & & & \\ & & GLJ_{12}^2 + 4EI_J_{12}^2 + 4EI_J_{22}^2 & GLJ_{11}^2 + 4EI_J_{11}^2 + 4EI_J_{12}^2 & \\ & & & GLJ_{11}^2 + 4EI_J_{11}^2 + 4EI_J_{12}^2 & \\ & & & & GLJ_{11}^2 + 4EI_J_{11}^2 + 4EI_J_{12}^2 & GLJ_{11}^2 + 4EI_J_{11}^2 + 4EI_J_{12}^2 & GLJ_{11}^2 + 4EI_J_{11}^2 + 4EI_J_{12}^2 & \\ & & & & & GLJ_{11}^2 + 4EI_J_{11}^2 + 4EI_J_{12}^2 & GLJ_{11}^2 + 4EI_J_{11}^2 + 4EI_J_{12}^2 & \\ & & & & & & GLJ_{11}^2 + 4EI_J_{11}^2 + 4EI_J_{12}^2 & \\ & & & & & & & \end{bmatrix}$$

When considering the distribution coefficient, it is not necessary to consider the coupling between the bending moments at the member end, but only the diagonal elements (rotational stiffness) of the stiffness matrix  $\mathbf{K}$  [4].

Therefore, the rotational stiffness of the member in the global coordinate system is:

$$\begin{cases} S_{ij}^x = \frac{1}{L} (GLJ_{11}^2 + 4EI_J_{12}^2 + 4EI_J_{22}^2) \\ S_{ij}^y = \frac{1}{L} (GLJ_{11}^2 + 4EI_J_{12}^2 + 4EI_J_{22}^2) \\ S_{ij}^z = \frac{1}{L} (GLJ_{11}^2 + 4EI_J_{12}^2 + 4EI_J_{22}^2) \end{cases}$$

The distribution coefficient is:  $\mu_{ij}^x = \frac{S_{ij}^x}{\sum S_{ij}^x}$ ;  $\mu_{ij}^y = \frac{S_{ij}^y}{\sum S_{ij}^y}$ ;  $\mu_{ij}^z = \frac{S_{ij}^z}{\sum S_{ij}^z}$

The distribution coefficients include bending moment distribution coefficients and torsional distribution coefficients. There are three groups of distribution coefficients at each rigid node, namely one group around the  $x$ -axis, one group around the  $y$ -axis, and one group around the  $z$ -axis. The sum of the distribution coefficients in each group is 1.

### Out-plane Stiffness $K_{out}$ (Three-dimensional calculation)

AECD is a CFST X-pillar with intersection B. Points C and E are sliding bearings. Points A and D are fixed bearings. A rigid body CE is connected between points C and E at the top of the pillar. The length of the CD is L. CB/CD=λ. The load of the pillar can be equivalent as shown in Figures 11 and 12.

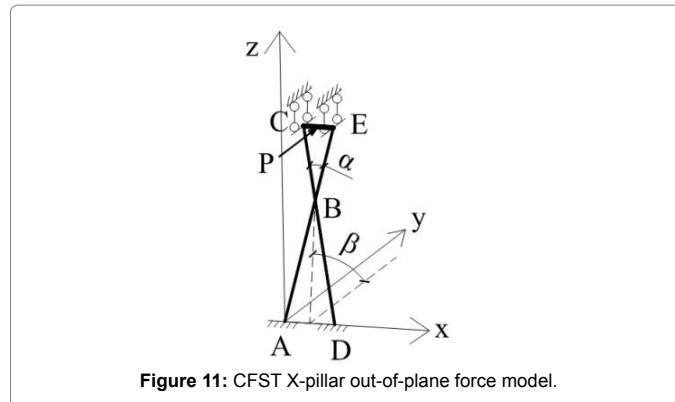


Figure 11: CFST X-pillar out-of-plane force model.

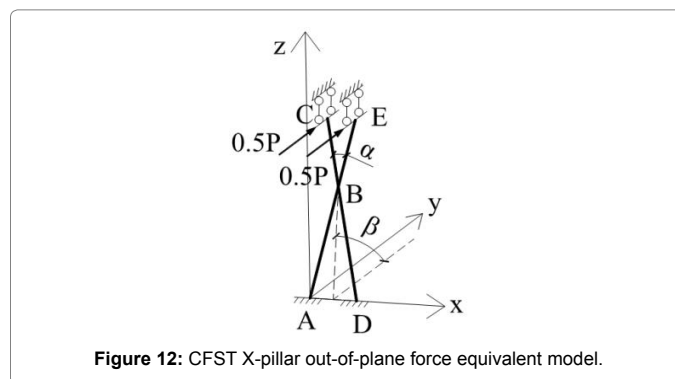


Figure 12: CFST X-pillar out-of-plane force equivalent model.

Due to the symmetrical structure of the CFST X-pillar, only half of the CFST X-pillars have been studied. As shown in the Figure 13, AB-BC is a CFST X-pillar calculation structure, in which point A is a fixed branch, and point C is a slip support that is movable only in the  $y$ -direction [5].

Define the local coordinate system of the AB member: Take the AB direction as the  $x'$  direction, and the direction perpendicular to  $x'$  to the left as the  $y'$  direction in the plane of the CFST X-pillar. And define the  $z'$  direction according to the right-handed spiral rule [6].

Define the local coordinate system of the BC member: Take the BC direction as the  $x''$  direction, and the direction perpendicular to  $x''$  to the left as the  $y''$  direction in the plane of the CFST X-pillar. And define the  $z''$  direction according to the right-handed spiral rule (Figure 14).

The relationship between the local coordinate system and the global coordinate system can be obtained through geometric relations [7].

$$\begin{cases} l_{11}^a = \sin \frac{\alpha}{2}; & l_{21}^a = \cos \frac{\alpha}{2} \cos \beta; & l_{31}^a = \cos \frac{\alpha}{2} \sin \beta; & l_{11}^b = -\sin \frac{\alpha}{2}; & l_{21}^b = \cos \frac{\alpha}{2} \cos \beta; & l_{31}^b = \cos \frac{\alpha}{2} \sin \beta \\ l_{12}^a = -\cos \frac{\alpha}{2}; & l_{22}^a = \sin \frac{\alpha}{2} \cos \beta; & l_{32}^a = \sin \frac{\alpha}{2} \sin \beta; & l_{12}^b = -\cos \frac{\alpha}{2}; & l_{22}^b = -\sin \frac{\alpha}{2} \cos \beta; & l_{32}^b = -\sin \frac{\alpha}{2} \sin \beta \\ l_{13}^a = 0; & l_{23}^a = -\sin \beta; & l_{33}^a = \cos \beta; & l_{13}^b = 0; & l_{23}^b = -\sin \beta; & l_{33}^b = \cos \beta \end{cases}$$

Using the previous torque distribution method, the internal force expression of the CFST X-pillar can be calculated. Finally, CFST X-pillar top displacement  $\Delta_{out}$  can be obtained by the method of graph multiplication under in-plane force  $P_{out}$ .

$$\Delta_{out} = \frac{L^2}{EI \left( \tan^2 \frac{\alpha}{2} + \cos^2 \beta \right)} (\Delta_B^p \eta_M \eta_A + P_{out} \eta_{out})$$

among them,

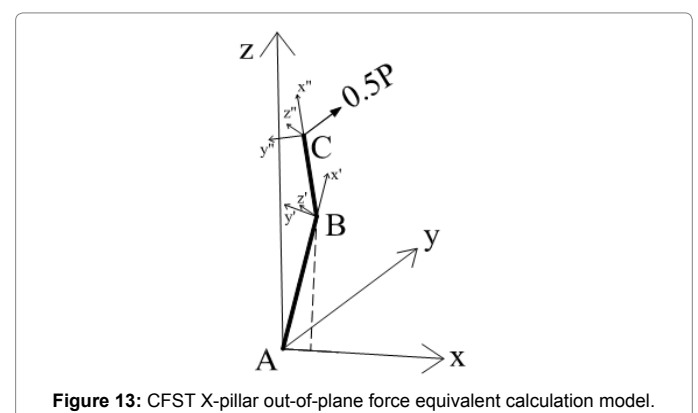


Figure 13: CFST X-pillar out-of-plane force equivalent calculation model.

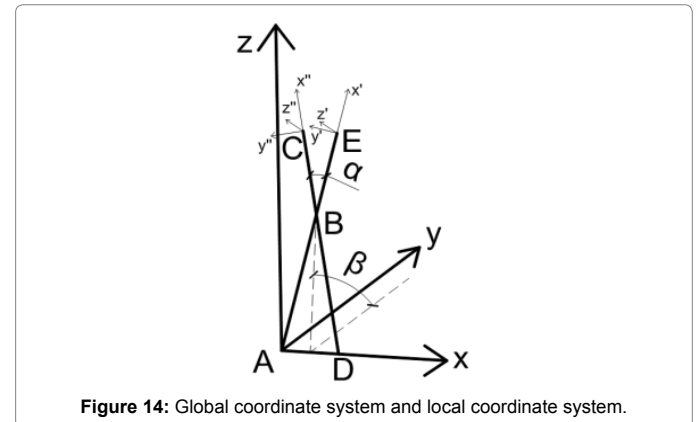


Figure 14: Global coordinate system and local coordinate system.

$$\eta_{\Delta} = \frac{1}{4}(1-\lambda)\lambda^2 \sin \frac{\alpha}{2} \sin \alpha \sin \beta \times \left( \cos^2 \beta \sin \alpha_1 + \tan \frac{\alpha}{2} \sin \frac{\alpha}{2} \sin \beta \right)$$

$$- \frac{1}{2}(1-\lambda)\lambda^2 \sin \beta \left( \cos \alpha + \frac{1}{2} \right) \left( \cos \frac{\alpha}{2} - \tan \frac{\alpha}{2} \sin \frac{\alpha}{2} \right) \left( \cos^2 \beta \sin \alpha_1 + \tan \frac{\alpha}{2} \sin \frac{\alpha}{2} \sin \beta \right)$$

$$+ \frac{1}{4}(1-\lambda)\lambda^2 \tan \frac{\alpha}{2} \sin \frac{\alpha}{2} \cos^2 \beta \left( -\sin \beta \sin \alpha_1 + 2 \tan \frac{\alpha}{2} \sin \frac{\alpha}{2} \right) + \frac{1}{6}(1-\lambda)\tan^2 \frac{\alpha}{2} \sin^2 \alpha \sin^2 \beta$$

$$+ \frac{1}{12}(1-\lambda)(1-3\lambda) \sin \beta (\cos \alpha - 2\lambda \cos \alpha - 1) \left( \cos \frac{\alpha}{2} + \tan \frac{\alpha}{2} \sin \frac{\alpha}{2} \right) \left( \cos^2 \beta \sin \alpha_1 + \tan \frac{\alpha}{2} \sin \frac{\alpha}{2} \sin \beta \right)$$

$$- \frac{1}{6}(1+3\lambda)(1-\lambda) \cos^2 \frac{\alpha}{2} \sin \beta \left( \cos \frac{\alpha}{2} + \tan \frac{\alpha}{2} \sin \frac{\alpha}{2} \right) \left( \cos^2 \beta \sin \alpha_1 + \tan \frac{\alpha}{2} \sin \frac{\alpha}{2} \sin \beta \right)$$

$$\eta_{\text{out}} = \eta_p \lambda L \sin \beta \cos^2 \beta \left[ \lambda^2 \left( -\frac{1}{2}\lambda + \frac{1}{3} \right) \left( \cos \alpha + \frac{1}{2} \right) \left( \cos \frac{\alpha}{2} + \tan \frac{\alpha}{2} \sin \frac{\alpha}{2} \right) - \frac{1}{48}(1-3\lambda)\lambda \sin \frac{\alpha}{2} \tan \frac{\alpha}{2} \right. \\ \left. + \frac{1}{32}(1-\lambda)(\cos \alpha - 2\lambda \cos \alpha - 1) \left( \cos \frac{\alpha}{2} - \tan \frac{\alpha}{2} \sin \frac{\alpha}{2} \right) \right] \\ + \lambda L \tan^2 \frac{\alpha}{2} \left[ \lambda^2 \left( -\frac{1}{2}\lambda + \frac{1}{3} \right) \left( \cos \alpha + \frac{1}{2} \right) \sin^2 \beta + \frac{1}{24}\lambda(1-3\lambda) \sin^2 \frac{\alpha}{2} \cos^2 \beta + \frac{1}{32}(1-\lambda)(\cos \alpha - 2\lambda \cos \alpha - 1) \cos \alpha \sin^2 \beta \right]$$

$$\text{So the in-plane stiffness is: } K_{\text{out}} = \frac{1}{\Delta_{\text{out}}}.$$

## Horizontal Load Distribution Calculation

The in-plane stiffness  $K_{\text{in}}$  is along the x-direction and the out-of-plane stiffness  $K_{\text{out}}$  is along the y-direction (Figure 15) [8]. The s-direction is an arbitrary direction, the angle between which and the y-direction is  $\varphi$ . When unit "1" displacement occurs in the s-direction, that is,  $\Delta=1$ , it can be decomposed into displacements in x and y directions.

$$\Delta_x = \sin \varphi, \Delta_y = \cos \varphi$$

The force generated along the s-direction under displacement is:

$$F_s = F_x \sin \varphi + F_y \cos \varphi = K_{\text{in}} \sin^2 \varphi + K_{\text{out}} \cos^2 \varphi$$

Suppose that there are n CFST X-pillars, and the stiffness of each CFST X-pillar is denoted by  $K_{\text{si}}$  ( $i=1,2,\dots,n$ ), which is numbered counterclockwise.

$$K_{\text{si}} = F_{\text{si}} = \frac{\sin^2 \varphi_i}{\Delta_{\text{in}}} + \frac{\cos^2 \varphi_i}{\Delta_{\text{out}}}$$

$$\varphi_i = \frac{2\pi(i-1)}{n}$$

The overall lateral stiffness of all CFST X-pillars is

$$K = K_{s1} + K_{s2} + \dots + K_{sn} = \frac{n}{2} \left( \frac{1}{\Delta_{\text{in}}} + \frac{1}{\Delta_{\text{out}}} \right)$$

When a horizontal force  $P$  acts vertically on the ring beam above

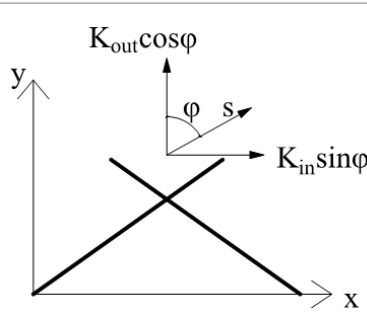


Figure 15: CFST X-pillar top view (stiffness).

the first CFST X-pillar, the horizontal force assigned by the i-th CFST X-pillar is given as (Figure 16):

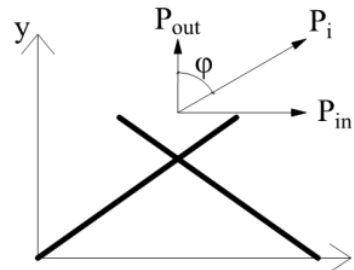


Figure 16: CFST X-pillar top view (horizontal load).

$$P_i = P \frac{K_{\text{si}}}{K} = P \left\{ 1 + \left( 1 - \frac{2}{\eta_k + 1} \right) \cos \left[ \frac{4(i-1)\pi}{n} \right] \right\}$$

$$\eta_k = \frac{\Delta_{\text{in}}}{\Delta_{\text{out}}}$$

Decomposes  $P_i$  into an in-plane load  $P_{\text{in}}$  and an out-of-plane load  $P_{\text{out}}$ .

$$P_{\text{in}} = P_i \sin \varphi_i = \frac{P}{n} \left\{ 1 + \left( 1 - \frac{2}{\eta_k + 1} \right) \cos \left[ \frac{4(i-1)\pi}{n} \right] \right\} \sin \left[ \frac{2(i-1)\pi}{n} \right]$$

$$P_{\text{out}} = P_i \cos \varphi_i = \frac{P}{n} \left\{ 1 + \left( 1 - \frac{2}{\eta_k + 1} \right) \cos \left[ \frac{4(i-1)\pi}{n} \right] \right\} \cos \left[ \frac{2(i-1)\pi}{n} \right]$$

$$\eta_k = \frac{\frac{\Delta_{\text{in}}}{P_{\text{in}}}}{\frac{\Delta_{\text{out}}}{P_{\text{out}}}} \tan \left[ \frac{2(i-1)\pi}{n} \right].$$

## CFST X-pillar Internal Force Expression under Horizontal Load

Here only the internal forces of the BC rod end are given:

- Under in-plane load  $P_{\text{in}}$

$$M_{\text{BC}}^{P_{\text{in}}, z} = -\frac{\eta_{\text{in}}(7-3\lambda)\lambda^2 L P_{\text{in}}}{4(1+3\lambda)} - \frac{(1-\lambda)^2 L P_{\text{in}}}{4 \cos \frac{\alpha}{2}}$$

$$\eta_{\text{in}} = \cos \frac{\alpha}{2} - \frac{(A\lambda^2 L^2 - 12I) \sin \frac{\alpha}{2}}{A\lambda^2 L^2 \tan \frac{\alpha}{2} + 12I \cot \frac{\alpha}{2}}$$

- Under out-of-plane load  $P_{\text{out}}$

$$M_{\text{BC}}^{P_{\text{out}}, x} = -\frac{2\Delta_B^P \eta_M (1-\lambda) \sin \frac{\alpha}{2}}{\tan^2 \frac{\alpha}{2} + \cos^2 \beta} \left( \cos^2 \beta \sin \alpha_1 + \tan \frac{\alpha}{2} \sin \frac{\alpha}{2} \sin \beta \right)$$

Among them,

$$\alpha_1 = \arccos \sqrt{\sin^2 \frac{\alpha}{2} + \cos^2 \frac{\alpha}{2} \cos^2 \beta}$$

$$\Delta_B^P = \frac{-\frac{(1-\lambda)P_{\text{out}}}{\sin \beta} - \frac{3}{4}\lambda P_{\text{out}} \left( \cos \frac{\alpha}{2} - \sin \frac{\alpha}{2} \tan \frac{\alpha}{2} \right) \left( \eta_p \cos^2 \beta + \tan \frac{\alpha}{2} \sin \frac{\alpha}{2} \sin \beta \right)}{\frac{2\eta_M}{L} \left( \cos \frac{\alpha}{2} + \tan \frac{\alpha}{2} \sin \frac{\alpha}{2} \right) \left( \cos \beta \sin \alpha_1 + \tan \frac{\alpha}{2} \sin \frac{\alpha}{2} \sin \beta \right)}$$

$$\eta_M = -\frac{6EI}{(1-\lambda)^2 L^2}$$

$$\eta_P = \left[ \sin\alpha_1 - \frac{(A\lambda^2 L^2 - 12I) \cos\alpha_1}{A\lambda^2 L^2 \cot\alpha_1 + 12I \tan\alpha_1} \right].$$

## CFST X-pillar Internal Force Expression under Gravity Load

The load of the pillar can be equivalent as shown in Figure 17.

Here only the internal forces of the BC rod end are given:

$$M_{BC}^{Gx} = \frac{-2\Delta_B^G \eta_M (1-\lambda) \sin\frac{\alpha}{2}}{\tan^2\frac{\alpha}{2} + \sin^2\beta} \left( \sin^2\beta \sin\alpha_2 + \tan\frac{\alpha}{2} \sin\frac{\alpha}{2} \cos\beta \right)$$

Among them,

$$\alpha_2 = \arccos \sqrt{\sin^2\frac{\alpha}{2} + \cos^2\frac{\alpha}{2} \sin^2\beta}$$

$$\Delta_B^G = \frac{(1-\lambda)G_i}{\cos\beta} - \frac{3}{4}\lambda G_i \left( \cos\frac{\alpha}{2} - \tan\frac{\alpha}{2} \sin\frac{\alpha}{2} \right) \left( \eta_G \sin^2\beta - \tan\frac{\alpha}{2} \sin\frac{\alpha}{2} \cos\beta \right)$$

$$- \frac{2\eta_M}{L} \left( \cos\frac{\alpha}{2} + \tan\frac{\alpha}{2} \sin\frac{\alpha}{2} \right) \left( \sin\alpha_1 \sin^2\beta + \tan\frac{\alpha}{2} \sin\frac{\alpha}{2} \cos\beta \right)$$

$$\eta_M = -\frac{6EI}{(1-\lambda)^2 L^2}$$

$$\eta_G = \sin\alpha_2 - \frac{(A\lambda^2 L^2 - 12I) \cos\alpha_2}{A\lambda^2 L^2 \cot\alpha_2 + 12I \tan\alpha_2}.$$

## X-pillar Total Internal Force Expression

Previously, the internal forces of the CFST X-pillar under horizontal loads (including in-plane and out-of-plane) and gravity loads have been calculated. They are  $M^{Pin}$ ,  $M^{Pout}$  and  $M^G$  respectively. And the total internal force expression is  $M = M^{Pin} + M^{Pout} + M^G$  [9].

Here only the internal forces of the BC rod end are given:

$$M_{BC}^{Gx} = -2\eta_M (1-\lambda) \sin\frac{\alpha}{2} \left[ \frac{\Delta_B^G}{\tan^2\frac{\alpha}{2} + \sin^2\beta} \left( \cos^2\beta \sin\alpha_1 + \tan\frac{\alpha}{2} \sin\frac{\alpha}{2} \sin\beta \right) + \frac{\Delta_B^G}{\tan^2\frac{\alpha}{2} + \sin^2\beta} \left( \sin^2\beta \sin\alpha_2 + \tan\frac{\alpha}{2} \sin\frac{\alpha}{2} \cos\beta \right) \right]$$

## Specific Project Optimization Examples

The cooling tower bottom radius is 70 meters and the height is 173 meters. The pillars used are concrete-filled steel tube X pillars. The steel pipe is Q420 steel. The concrete strength grade is C60 and the shell

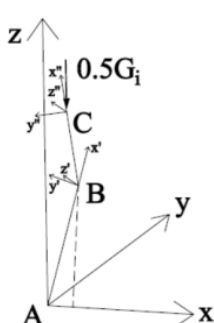


Figure 17: Calculation model of CFST X-pillar under gravity load.

concrete grade is C60 (Figure 18).

The height of the CFST X-pillar is  $H=30$  m, then the length of the corresponding CFST X-pillar is  $L = \frac{30}{\sqrt{\cos^2\alpha + \sin^2\beta}}$ . And the number of CFST X-pillars is  $n=44$ . The equivalent static wind load  $P=6155$  kN, and the total gravity load of the ring beam and superstructure is  $G=419832$  kN. The outer diameter of the CFST X-pillar section is  $D=1000$  mm, the thickness of the steel tube is  $t=20$  mm, and the combined elastic modulus  $E_{sc}=5.245 \times 10^4$  N/mm<sup>2</sup> [10].

- Optimization result of  $\alpha$

It can be seen that the stress reaches the minimum when  $\alpha=76^\circ$ . Considering the calculation error, the optimal value range of cross angle  $\alpha$  is  $17^\circ \sim 23^\circ$  (Figures 19 and 20).

- Optimization result of  $\beta$

It can be seen that the stress reaches the minimum when  $\beta=76^\circ$ . Considering the calculation error, the optimal value range of slope angle  $\beta$  is  $73^\circ \sim 79^\circ$  (Figures 21 and 22).

- Optimization result of  $\lambda$

It can be seen that the stress reaches the minimum when  $\lambda=0.32$ . Considering the calculation error, the optimal value range of determining the node ratio  $\lambda$  is  $0.29 \sim 0.35$  (Figures 23 and 24).

## Conclusion

The position of the intersection point is better above the middle of CFST pillar, the range of ratio  $\lambda$  is  $0.2 \sim 0.35$ ; the optimal value of

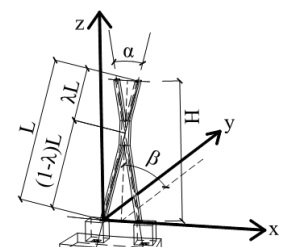


Figure 18: CFST X-pillar configuration parameters.

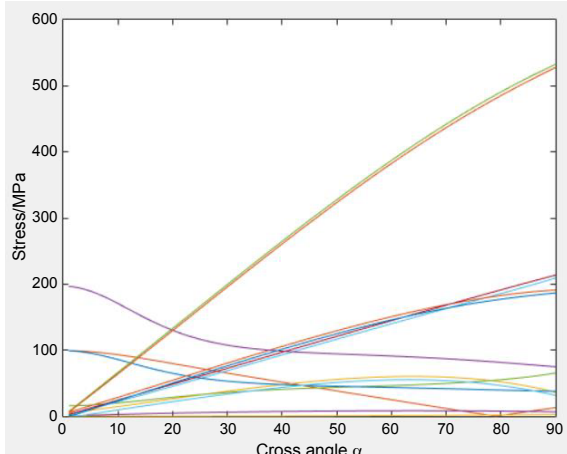
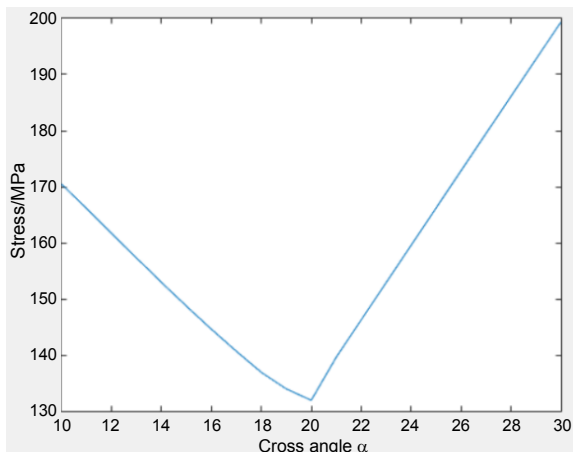
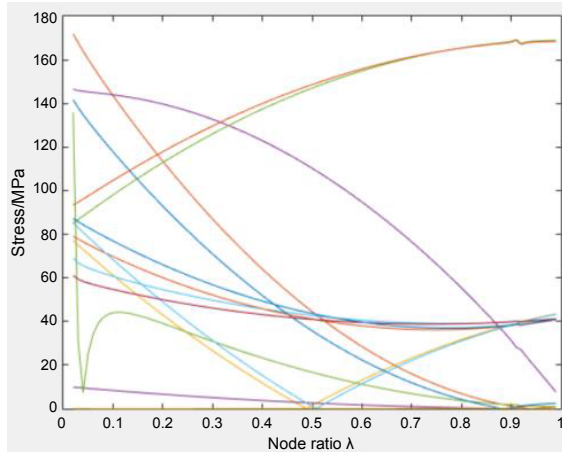


Figure 19: Cross angle  $\alpha$ -stress relationship diagram.



**Figure 20:** Cross angle  $\alpha$ -stress relationship envelope diagram.



**Figure 23:** Node ratio  $\lambda$ -stress relationship diagram.

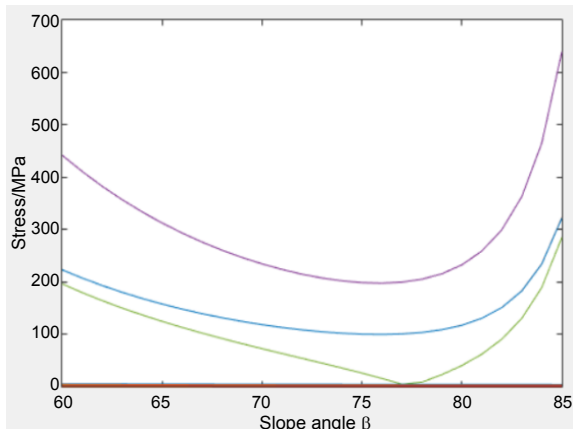


**Figure 21:** Slope angle  $\beta$ -stress relationship diagram.

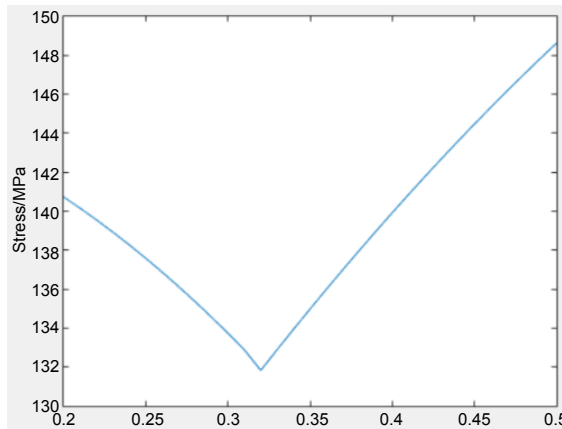


**Figure 24:** Node ratio  $\lambda$ -stress relationship envelope diagram.

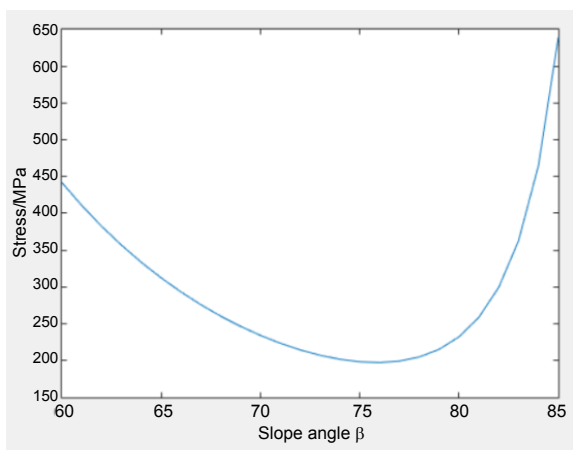


**Figure 22:** Slope angle  $\beta$ -stress relationship envelope diagram.

cross angle  $\alpha$  is  $18^\circ \sim 22^\circ$ ; the optimal range of CFST pillar tilt angle  $\beta$  is  $74^\circ \sim 78^\circ$ .

## References

1. Yuqiu L, Shihua B, Wenqi K (2012) Structural Mechanics I. Beijing, China: High Education Press.

2. Xi-Ling MA, Yang QL (2001) Moment Distribution Method for non Linear Joint Displacement Space Rigid Frames.
3. Lin-Hai H, Jingshi H, Yong CW (2007) Behavior of Steel Beam to Concrete-Filled Steel Tubular Column Connections after Exposure to Fire. *Journal of Structural Engineering*, 133.
4. Liu JL (2010) Preventing progressive collapse through strengthening beam-to-column connection, Part 1: Theoretical analysis. *Journal of Constructional Steel Research* 66: 229-237.
5. Fu YY, Yan SW, Du C (2011) Performance Analysis of CFST Column and RC Column Subjected to Eccentric Load. *Applied Mechanics and Materials* 94: 805-809.
6. Xiong W, Wu MZ (2005) Truss optimization design of truss string structure. *Journal of Xi'an University of Architecture & Technology*.
7. Liqian X, Dianjian H (2014) Advanced Engineering and Technology. *Proceedings of the 2014 Annual Congress on Advanced Engineering & Technology*.
8. Shen ZY, Li GQ, Chan SL (2005) Advances in Steel Structures 1: 395-401.
9. Haiyang W, Xiaoxiong Z, Yixiang L, Chaoning L, Chi KI (2007) Study of recycled concrete-filled steel tubular columns on the compressive capacity and fire resistance. *Advances in Mechanical Engineering*, 9.
10. Kodur VKR (1995) Performance-based fire resistance design of concrete-filled steel columns. *Journal of Constructional Steel Research* 51: 21-36.